Research article

Experimental of buckling restrained brace hysteretic performance with carbon fiber wrapped in concrete

Yuan Fang[1], Lei Lv[2], Yuqiang Gao[3], Zhongqiu Fu[4]

Abstract: Buckling restrained brace is an important structure for improving the seismic resistance of structures. Conducting research on new types of buckling restrained brace can improve the seismic performance and reliability of buckling resistant support. Four different types of buckling restrained braces specimens were designed and manufactured: cross-shaped square steel pipe members, cross-shaped round steel pipe members, cross-shaped carbon fiber members, and in-line carbon fiber members. By conducting quasi-static tests, the force displacement hysteresis curves, skeleton curves, stiffness degradation, equivalent viscous damping coefficient, and energy dissipation ratio of four different types of buckling restrained brace were analyzed. The research results showed that all four buckling restrained brace specimens have good hysteresis performance. The load-bearing capacity and energy consumption performance of the three specimens of square steel pipe, round steel pipe and carbon fiber with the same core unit are the same, but the inline type is worse than the cross type. The core unit specimen with a width of 80 mm is about 60% higher in bearing capacity and energy consumption than a specimen with a width of 50 mm. The core unit of some specimens undergoes multi-wave buckling. For carbon fiber specimens, the CFRP is prone to breakage due to the lateral thrust of the restraining unit. Therefore, steel hoop or stirrup should be added to the end to improve the restraint effect when designing and manufacturing.

Keywords: carbon fiber, light aggregate concrete, hysteretic behavior, hysteretic curve, damping coefficient

---

[1]ME., Department of Architecture and Civil engineering, Zhejiang Tongji Vocational College of Science and Technology, Hangzhou 311231, China, e-mail: fangyuan19881025@126.com, ORCID: 0009-0006-0561-3289

[2]ME., Department of Architecture and Civil engineering, Zhejiang Tongji Vocational College of Science and Technology, Hangzhou 311231, China, e-mail: lvlei19841125@126.com, ORCID: 0009-0007-7735-2476

[3]PhD student, College of Civil and Transportation Engineering, Hohai University, Nanjing 210098, China, e-mail: 201304040003@hhu.edu.cn, ORCID: 0009-0005-7964-9594

[4]Prof., PhD., College of Civil and Transportation Engineering, Hohai University, Nanjing 210098, China, e-mail: fuzhongqiu@hhu.edu.cn, ORCID: 0009-0002-2538-9967

1. Introduction

The sudden and destructive earthquake seriously threatens the safety of people 's lives and property, and has become one of the important natural disasters that affect human life and hinder economic development. The unpredictability of earthquakes determines that the destruction of earthquakes can only be reduced by improving the seismic performance of buildings at this stage [1]. As a new type of metal yielding energy dissipation brace, buckling restrained brace (BRB) has been widely used in the seismic design of existing structures and new structures around the world in recent years because of its clear mechanical principle and stable hysteretic performance [2].

After the Hanshin earthquake in Japan and the Northridge earthquake in the United States, countries such as Japan and the United States first proposed buckling-restrained braces composed of energy-consuming inner cores and external constraints. Scholars around the world have also carried out a lot of theoretical and experimental researches on the structural working principle, energy dissipation performance, optimization and improvement of buckling-restrained braces [3]. Miller et al. [4] proposed a self-centering buckling-restrained brace using a super-elastic memory alloy column and carried out related tests. The results show that the hysteresis curve of the cylindrical memory metal self-centering buckling-restrained brace has better hysteretic performance and energy dissipation capacity than the ordinary buckling-restrained brace. Kim et al. [5] conducted a comparative test on two kinds of H-shaped steel inner-core buckling-restrained braces. The results show that the H-shaped buckling-restrained brace with square steel tube has better economy and energy dissipation performance. Chou et al. [6] developed a new steel dual-core self-centering brace (DC-SCB) and conducted related research. The results showed that the axial deformation capacity of the brace is doubled by serial deformations of two sets of tensioning elements arranged in parallel. Wu et al. [7] compared and analyzed the seismic performance of buckling restrained braces under different constraint ratios, and obtained the law that when the constraint ratio increased, the influence of the outer sleeve on the seismic performance of the brace decreased instead. Guo et al. [8–10] carried out research on all-steel assembled buckling-restrained braces, proposed a variety of new cross-section forms, and carried out theoretical derivation and numerical simulation analysis on the design of the peripheral constraint ratio and peripheral connection of the brace. A double inner-core buckling-restrained brace connected with wavy webs is also proposed and tested. The results show that the bending stiffness of the overall peripheral constraints and the strength of the inner core end of the component under this structure are greatly improved. Jia et al. [11] proposed carbon fiber buckling-restrained brace and conducted loading tests. It was found that increasing the area of the core section can effectively increase the ability of the connection section of the buckling-restrained brace to resist bending moment and prevent local buckling instability due to sudden change of stiffness. From the above research, it can be seen that the existing research mainly focuses on the research of traditional concrete-filled steel tube restrained, all-steel or self-centering buckling-restrained braces. There are relatively few studies on the new buckling-restrained braces with external restraint and carbon fiber cladding, and the influence of external restraint type and gap on seismic performance is rarely involved. Therefore, it is of great significance to carry out the seismic test research of the new type of buckling restrained brace to improve the seismic performance and reliability of the buckling restrained brace.

In order to explore the seismic performance of buckling-restrained braces under different cross-section types and different gaps, four different types of buckling-restrained braces are designed and manufactured in this paper, which are cross-shaped concrete-filled square steel tubular members, cross-shaped concrete-filled circular steel tubular members, cross-shaped carbon fiber reinforced concrete members, and one-shaped carbon fiber reinforced concrete members. Each group is divided into three specimens with different inner core sizes and gaps, and its performance test is carried out. Through the comparative analysis of the test results, it provides a basis for the engineering application and design of the new buckling-restrained brace.

2. Experiment framework

2.1. Specimen

As shown in Fig. 1–4, four groups of buckling restrained braces with different restraint forms were designed in the experiment (BRB-A~BRB-D). BRB-A: the external restraint is square concrete filled steel tubular members, the core unit adopts a cross section; BRB-B: the core unit adopts a cross section, the outer constraint is a circular steel tube concrete member; BRB-C: the core material is I-shaped steel, the constraint member is lightweight aggregate concrete, and two layers of carbon fiber cloth are wrapped in lightweight aggregate concrete. BRB-D: the external constraint is two layers of carbon fiber cloth confined concrete members, the core unit adopts a cross section. Each group is divided into three specimens based on the size of the core unit. The size of buckling restrained braces are shown in Table 1, and the geometry of specimens are shown in Fig. 1–4.
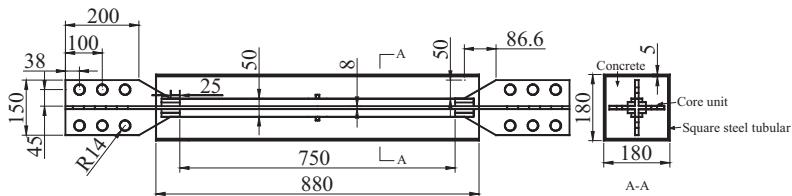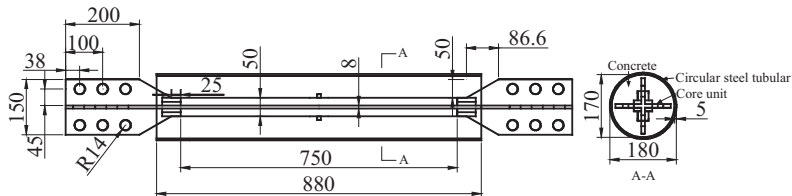

Fig. 1. Geometry of specimen BRB-A
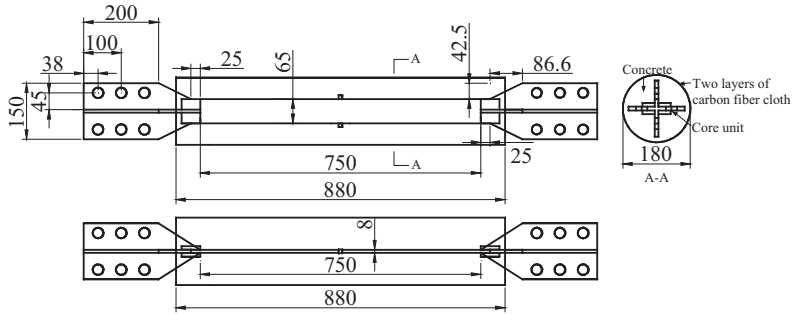

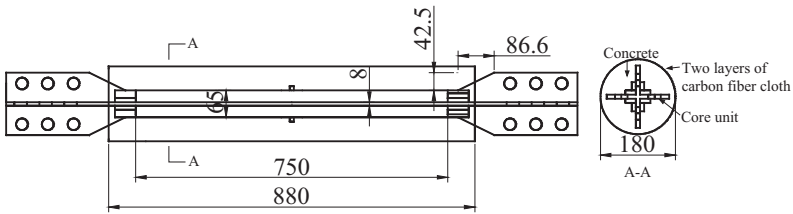Fig. 2. Geometry of specimen BRB-B

Fig. 3. Geometry of specimen BRB-C

Fig. 4. Geometry of specimen BRB-D

Table 1. Size of buckling restrained braces

Cross section Type	Specimen	Core unit			Constraint			Silicone interlayer [mm]	Theoretical yield force [kN]
		Length [mm]	Outer diameter or width [mm]	Thickness [mm]	Length [mm]	Outer diameter or width [mm]	Thickness [mm]		
BRB-A	A1	750	50	8	880	180	5	2	191.36
	A2		65					2	253.76
	A3		80					1	316.16
BRB-B	B1	750	50	8	880	180	5	1	191.36
	B2		65					1	253.76
	B3		80					2	316.16
BRB-C	C1	750	65	8	880	180	–	2	135.20
	C2		65					1	135.20
	C3		80					1	166.40
BRB-D	D1	750	65	8	880	180	–	2	253.76
	D2		65					1	253.76
	D3		80					1	316.16

2.2. Material parameter

1. Mechanical properties of lightweight aggregate concrete
   When making the specimen, lightweight aggregate concrete is selected as the filler between the core unit and the external constraint. The lightweight aggregate concrete is composed of coarse aggregate with gravel particle size of 1–3 mm, fine aggregate with fineness modulus of 2.8, P.C 32.5 composite Portland cement and water. In order to measure the compressive strength and elastic modulus of lightweight aggregate concrete, three 150×150×150 mm cube test blocks were made according to the Chinese standard GB/T50081-2019 for cube compression testing. The mechanical properties of lightweight aggregate concrete are shown in Table 2.

Table 2. Mechanical properties of lightweight aggregate concrete

Specimen	Elastic modulus E_c [GPa]	Poisson's ratio υ	Cube crushing strength f_{cu} [GPa]
1	23.6	0.17	0.0312
2	23.8	0.18	0.0316
3	24.2	0.17	0.0314
Mean	23.9	0.17	0.0314

2. Mechanical properties of steel
   In order to determine the probable mechanical properties of the steel in the specimen, the standard specimen is processed according to the relevant requirements of the national standard [12] 'Metallic Materials Room Temperature Tensile Test Method' (GB / T228-2002). The tensile strength, elastic modulus and Poisson's ratio of the steel are determined by the standard tensile test are shown in Table 3 below.

Table 3. Mechanical properties of steel

Specimen	Thickness [mm]	Yield strength f_y [GPa]	Tensile strength f_u [GPa]	Elastic modulus E_s [GPa]	Poisson's ratio υ
1	8	0.268	0.396	203	0.263
2	8	0.252	0.373	204	0.281
3	8	0.258	0.389	208	0.284
Mean	–	0.260	0.386	205	0.276

3. Mechanical properties of carbon fiber
   Carbon fiber cloth is provided directly by the manufacturer. The mechanical properties are shown in Table 4.

Table 4. Material properties of carbon fiber cloth

Material	Standard value of tensile strength [GPa]	Tensile modulus of elasticity [GPa]	Elongation [%]	Bending strength [GPa]	Interlaminar shear strength [GPa]	Mass per unit area [g/cm^2]	Thickness [mm]
Carbon fiber	3.682	228	1.57	0.635	0.0386	398	0.167

2.3. Test loading and measuring point arrangement

1. Test device

   The quasi-static loading was carried out on the MTS hydraulic servo system, the test device is shown in Figure 5. The tension and compression load range of the action head is –2500 kN ~+2500 kN, where tension is '+' and compression is '–'.

Fig. 5. Test device

2. Loading method

   The loading method adopts displacement control, which is determined by the micro-strain of 3% of the length of the specimen core unit. The loading range is –24 mm ~+24 mm, or until the specimen is destroyed and reaches the measurement range of the MTS hydraulic servo system, the loading is stopped. The loading process is shown in Table 5.

3. Measuring point arrangement

   During the test, to collect the strain change of the core unit under the action with hysteresis force, a three-dimensional strain gauge was arranged at the center of the two ends 50 mm away, and a two-dimensional strain gauge was arranged at the center of the middle, As shown in Fig. 6a. Similarly, a one-way strain gauge was arranged at the

center of the constraint unit 100 mm from the two ends, and a three-way strain gauge was arranged at the center of the middle, As shown in Fig. 6b. Considering that the connection between MTS hydraulic servo system, fixture, and specimens may have some clearance, which affects the accuracy of axial displacement data, two displacement sensors were placed symmetrically on the upper and lower connecting plates to obtain the real axial displacement, As shown in Fig. 6c.
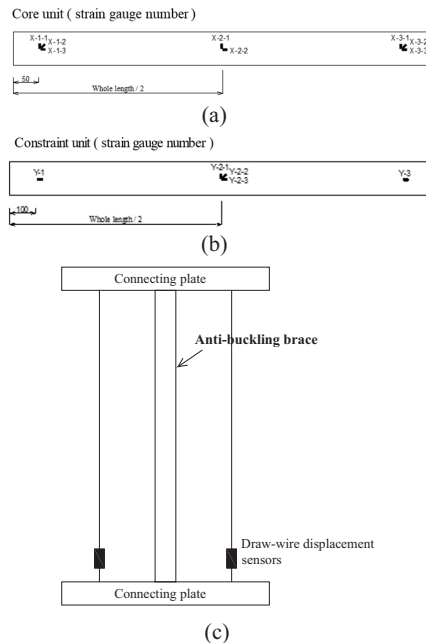

Fig. 6. Measuring points arrangement: a) Measuring points on the core unit, b) Measuring points on the constraint unit, c) Displacement sensors arrangement

Table 5. Loading method of buckling restrained brace specimens

Load step	Target strain amplitude of core yield section [%]	Axial displacement amplitude of core yield section [mm]	Number of cycles (c)
1	0.27	2	1
2	0.53	4	1
3	0.80	6	1
4	1.07	8	1
5	1.33	10	1
6	1.60	12	1
7	1.87	14	1
8	2.13	16	2

3. Results and analysis

3.1. Hysteretic curve

Figure 7–10 are the hysteresis curves of four buckling restrained brace specimens. The experimental results show that the hysteresis curves of the four buckling restrained brace specimens are full and stable, the hysteresis curves almost coincide under the same loading displacement. In the initial stage of tension and compression loading, the hysteresis curve changes in a straight line and maintains a constant stiffness, showing good hysteresis performance and deformation ability.
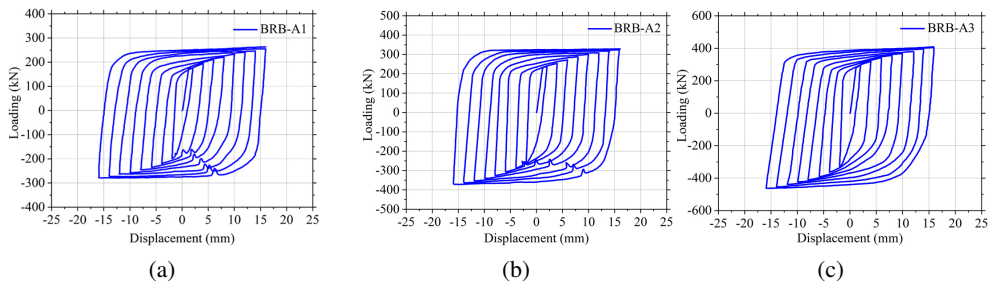

(a)	(b)	(c)

Fig. 7. Hysteresis curve of BRB-A specimens

(a)	(b)	(c)
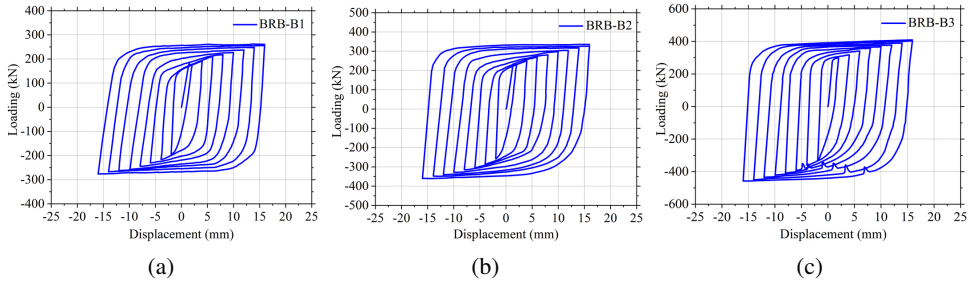
Fig. 8. Hysteresis curve of BRB-B specimens

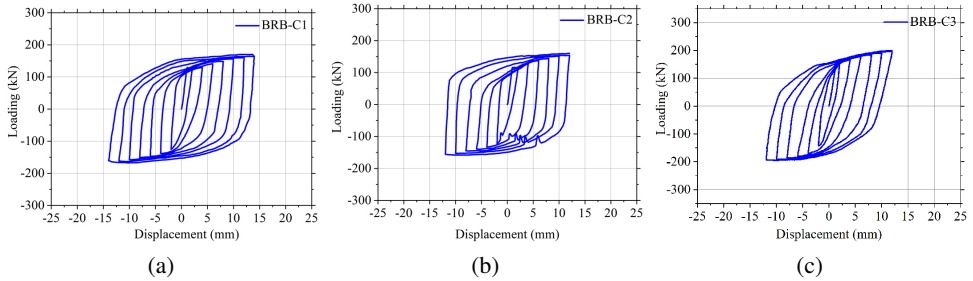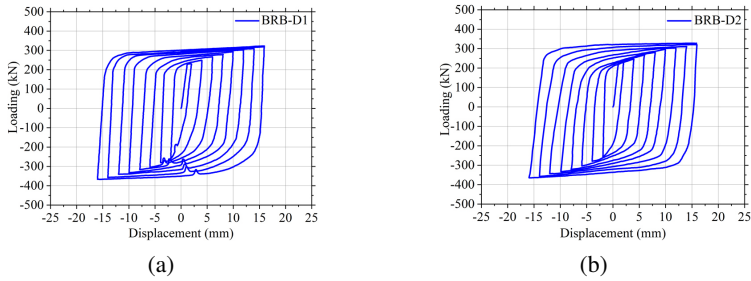|		
(a)	(b)	(c)

Fig. 9. Hysteresis curve of BRB-C specimens

Fig. 10. Hysteresis curve of BRB-D specimens

Figure 10 is the hysteretic curve of the carbon fiber confined lightweight aggregate concrete buckling restrained brace with cross steel core. It can be observed from the diagram that the specimen with a core diameter of 80 mm (BRB-D3), in the course of loading the compressive load displacement from 8 mm to 10 mm, the loading end lightweight aggregate concrete cracks, which leads to the fracture of the end carbon fiber cloth. For the phenomenon that the end restraint of the carbon fiber restraine buckling restrained brace is prone to the fracture of the carbon fiber cloth during the loading process, the steel hoop ring can be added to the end to improve the restraint effect of the end.

The specimens A1, A2, B3, C2, and D1 did not undergo overall instability failure, but their hysteresis curves "jumped" significantly in the compression stage, indicating that multi-wave buckling occurred at the yield section of the core element of the specimen. With the development of low-order buckling to high-order buckling, the filled concrete in the tube will be gradually crushed, and when the maximum deformation of the high-order buckling inner core is in contact with the outer steel tube, the lateral constraint can be maintained. This constraint mechanism can effectively prevent the core element of the inner core yield section from high-order buckling to local buckling failure. This high-order buckling phenomenon is the intrinsic nature of BRB to achieve compressive yield strengthening without overall or local buckling of the member [13].

3.2. Skeleton curve

Figure 11 shows the skeleton curves of four buckling restrained brace specimens. It can be seen that there are obvious turning points between the elastic stage and the yield stage of the four buckling restrained brace specimens, showing a typical double-fold line type, indicating that the four buckling restrained brace specimens have significant stiffness degradation characteristics and good deformation ability.

Comparing the compressive and tensile yield stages of the hysteresis curves of the four specimens, the tensile and compressive bearing capacity is different, and the compressive section is strengthened. Taking the core unit 80 mm square steel pipe anti buckling support specimen (BRB-A3) as an example, under a deformation rate of 1/88, the compressive bearing capacity is 462.6 kN, the tensile bearing capacity is 400.8 kN, and the ratio of compression to tension reaches 1.15. The reason is that the Poisson's ratio effect causes the BRB-A3

(a) BRB-A   (b) BRB-B   (c) BRB-C
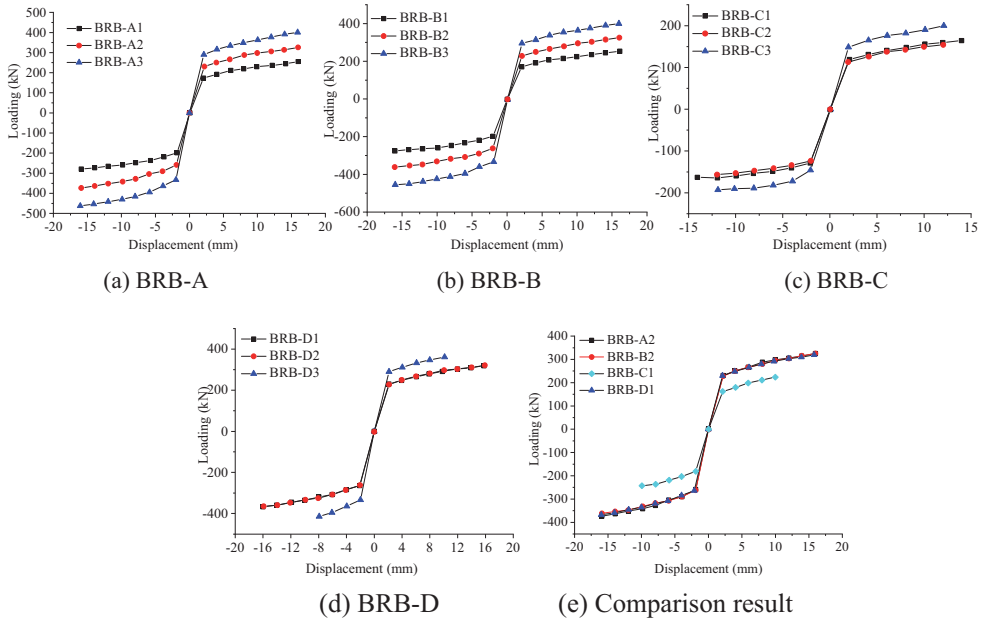
(d) BRB-D   (e) Comparison result

Fig. 11. Skeleton curve of specimens

core element to expand horizontally during compression, while the outer square steel tube constrains its deformation so that the core element is in a three-dimensional compression state. In addition, the concrete in the middle of the inner core can bear part of the axial force when it is compressed, which reduces the actual force of the steel, but has no effect when it is tensioned. Therefore, the bearing capacity of the specimen in the compression stage is higher than that in the tension stage, and the strengthening phenomenon occurs.

Compared with the specimens of the same section type, the larger the width of the core element, the higher the corresponding bearing capacity. Taking the buckling restrained brace specimen with circular steel tube (BRB-B) as an example, the tensile bearing capacity of the core unit component with a width of 50 mm is 253.0 kN, and the core unit component with a width of 80 mm is 400.0 kN, which increases about 58.1%. The compressive bearing capacity of the core unit component with a width of 50 mm is 275.1 kN, and the core unit component with a width of 80 mm is 454.8 kN, which increases about 65.3%. It can be seen that increasing the width of the core unit can significantly improve the overall stiffness of the specimen.

Figure 11e is the skeleton curve comparison diagram of buckling restrained brace specimens with different section types and carbon fiber restrained buckling restrained brace specimens with different core materials. The skeleton curves of three different types of buckling restrained brace specimens (BRB-A2, BRB-B2, BRB-D1) are basically coincident. Before loading to about 2 mm, the members are in the stage of elastic strain. With the increase of loading displacement, the members yield in the positive and negative directions, and the tensile and compressive bearing capacity can reach 300 kN. The above analysis shows that the external constraint element has no effect on its bearing capacity and stiffness performance. The skeleton

curve of the specimen (BRB-C1) with carbon fiber as the outer constraint and steel as the core material is significantly lower than that of the other three specimens. It shows that the bearing capacity and overall stiffness of the specimen (BRB-C1) with one-shaped steel core are worse than those of the cross-shaped (BRB-D1).

3.3. Stiffness degradation

The secant stiffness can reflect the variation of stiffness during the loading process of the specimens. The calculation formula is as follows:

$$(3.1) \qquad K_j^i = \frac{\left|+V_j^i\right| + \left|-V_j^i\right|}{\left|+\Delta_j^i\right| + \left|-\Delta_j^i\right|}$$

where: K_j^i – the secant stiffness of the i-th circle when the loading stage is j, V_j^i – load values at the i-th forward and reverse peak points, Δ_j^i – the displacement value of the i-th forward and reverse peak points.

The sectional stiffness of buckling restrained brace specimens with four sections was calculated according to the above formulas, the results were shown in Fig. 12. According to Fig. 12, with the increase of loading displacement, the secant stiffness of each specimens gradually decreases and eventually maintains near 20 kN/mm. Due to the collapse of the carbon fiber sheets at the periphery of specimen D3 when loaded to 8 mm, the secant stiffness only develops to around 50 kN/mm. Although the law of stiffness degradation is basically the same, there are differences in the stiffness values under the same displacement, which are mainly related to the frictional connection effect and the time when the anti-buckling supports enter buckling, and also related to the symmetry of the structure and supports. This phenomenon shows that buckling restrained braces can increase stiffness under small displacement, decrease equivalent stiffness under large displacement and increase energy consumption, which is conducive to reducing earthquake action [14, 15].

Comparing the buckling restrained brace specimens with different core unit diameters, the specimens with larger diameters have larger initial secant stiffness. As the loading displacement continues to increase, the difference in secant stiffness between the two gradually decreases, and ultimately the secant stiffness values of the two tend to overlap. Due to the influence of different cross-sectional areas and initial defects of buckling restrained brace specimens, the initial stiffness of each specimen of BRB-A and BRB-B types is different. However, carbon fiber constrained specimens (BRB-C1 and BRB-C2, BRB-D1 and BRB-D2) with the same width of core material and different gaps have very little difference in initial secant stiffness, and the trend is basically the same with displacement development. Therefore, it can be seen that the secant stiffness of the buckling restrained brace with carbon fiber is independent of the gap.

Figure 12e shows the comparison of secant stiffness between buckling restrained brace specimens with different cross-sectional types and carbon fiber constrained buckling restrained brace specimens with different core materials. Three types of buckling restrained braces with different constrained conditions (BRB-A2, BRB-B2, BRB-D1) exhibit significant stiffness

(a) BRB-A   (b) BRB-B   (c) BRB-C
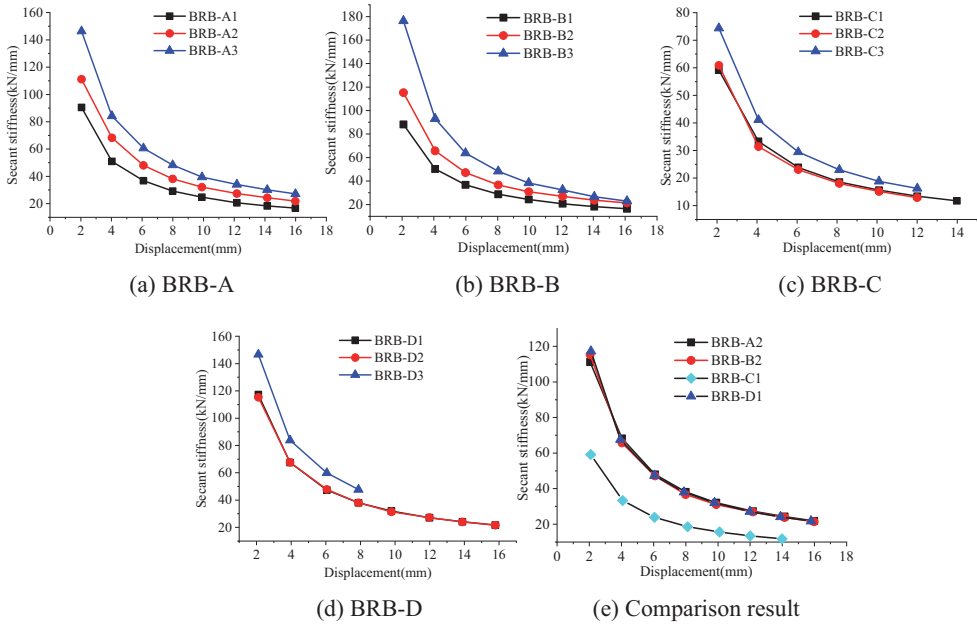
(d) BRB-D   (e) Comparison result

Fig. 12. Secant stiffness of specimens

degradation during the loading process, with a consistent trend towards 20 kN/mm, which indicates that the constrained types have no effect on the stiffness variation of the specimens. For the specimen BRB-C1 with a straight section steel as the core material, its secant stiffness curve is significantly lower than the specimens with other three types of cross section steel. The load-bearing capacity and stiffness of carbon fiber restrained buckling restrained brace with a straight section steel core are poor.

3.4. Cumulative energy consumption

The cumulative energy consumption of buckling restrained brace can be calculated by the following formula:

$$(3.2) \qquad\qquad W = \pi^2 EI\mu$$

where: W – cumulative energy consumption, E – elastic modulus, I – second moment of area, μ – Plastic dissipation coefficient.

Figure 13 shows the cumulative energy consumption of four types of buckling restrained brace specimens. Fig. 13a shows the buckling restrained brace specimens of square steel tubes with different core unit diameters. It can be seen from the figure that when the displacement of the specimens reach 14 mm, the cumulative energy consumption area of BRB-A3 reaches 67604 kN•mm, which is about 1.16 times that of BRB-A2 and 1.57 times that of BRB-A1. The cumulative energy consumption area of BRB-B3 reaches 71048 kN•mm, which is

approximately 1.26 times that of BRB-B2 and 1.63 times that of BRB-B1. Under the condition of satisfying overall stability, the diameter of the core unit is the determining factor affecting the energy consumption capacity of the specimen. For the carbon fiber constrained buckling restrained brace specimens (BRB-C, BRB-D), the cumulative energy consumption curves basically overlap, indicating that the core unit diameter has no effect on the energy consumption performance of the carbon fiber constrained buckling restrained brace specimens.
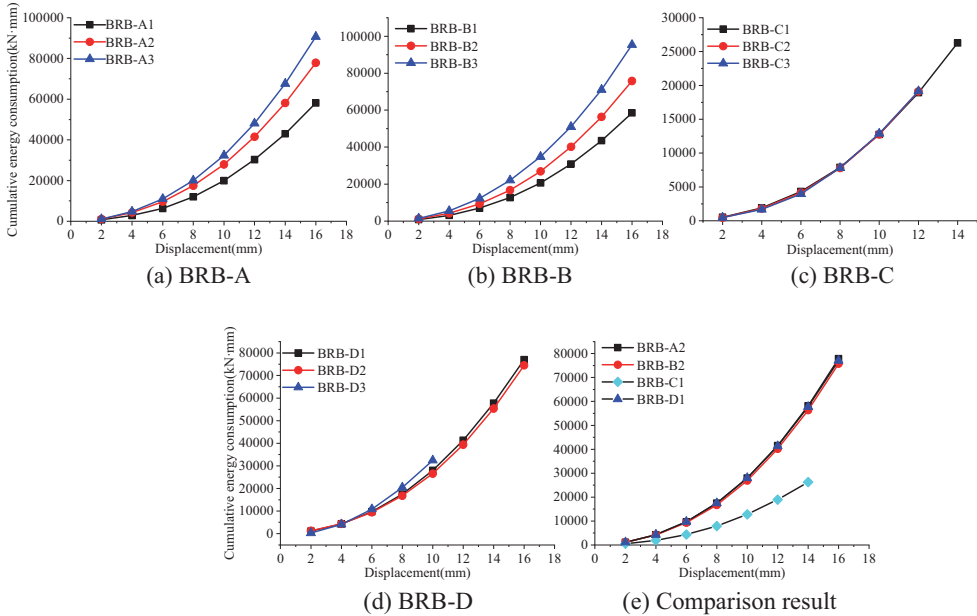

(a) BRB-A (b) BRB-B (c) BRB-C

(d) BRB-D (e) Comparison result

Fig. 13. Accumulated energy consumption

Based on the "bouncing" phenomenon of the hysteresis curve in Section 3.1, it can be inferred that whether the specimen has undergone significant multi wave buckling is the main factor affecting the energy dissipation capacity of the specimen The specimens with 2 mm partitions (BRB-A1, BRB-A2, BRB-B3, BRB-C1, BRB-D1) exhibit more significant multi wave buckling behavior and slightly weaker hysteresis energy dissipation ability compared to specimens with 1 mm partitions.

4. Conclusions

In this paper, quasi-static tests are carried out on four different types of buckling restrained brace specimens, the force displacement hysteresis curves, skeleton curves, stiffness degradation, equivalent viscous damping coefficient, and energy dissipation ratio of four different types of buckling restrained brace were analyzed. The conclusions are as follows:

1. The buckling restrained brace specimens with square steel pipe, round steel pipe, and carbon fiber have good hysteretic energy consumption. For different types of buckling restrained brace, when the same core unit is used, the load-bearing capacity and energy dissipation performance of the components are basically the same, and there is basically no impact on the energy dissipation of the inner core.

2. The core unit of a 2 mm spacer specimen undergoes significant multi-wave buckling under compression. It is shown that the obvious multi-wave buckling of the specimens is the main factor affecting the energy consumption of the specimens.

3. The load-carrying capacity and energy dissipation of I-shaped carbon fiber restrained buckling restrained brace specimens are poor. The test data shows that the load-carrying capacity and energy consumption of specimens with 80 mm width core unit are about 60% higher than that of 50 mm width members.

4. The core elements of some buckling restrained brace specimens undergo multi-wave buckling. For carbon fiber reinforced lightweight aggregate concrete buckling restrained brace specimens, the lateral thrust of the restraining element can cause the carbon fiber cloth to fracture. When designing and manufacturing, it should be considered to add steel hoops or stirrups at the ends to improve the constraint effect of the ends.

References

[1] Y. Li, J. Li, T. Guo, et al., "Bearing capacity and seismic performance of Y-shaped reinforced concrete bridge piers in a freeze-thaw environment", *Archives of Civil Engineering*, vol. 69, no. 1, pp. 367–384, 2023, doi: 10.24425/ace.2023.144178.

[2] Y. Zhou, W. Tian, and Y. Xiao, "Design recommendations for self-centering buckling restrained braces", *Engineering Structures*, vol. 273, no. 15, art. no. 115019, 2022, doi: 10.1016/j.engstruct.2022.115019.

[3] L. Peng, "Research on the energy dissipation of new all-steel buckling restrained brace", M.A. thesis, Hunan University, 2018.

[4] D. Miller and L. Fahnestock, "Self-centering buckling restrained braces for advanced seismic performance", in *Proceedings of the 2011 Structures Congress*. ASCE, 2011, pp. 960–970, doi: 10.1061/41171(401)85.

[5] H. Kim, H. Lee, and K. Ju, "Subassemblage test of buckling restrained braces with H-shaped steel core", *The Structural Design of Tall and Special Buildings*, vol. 24, no. 4, pp. 243–256, 2015, doi: 10.1002/tal.1164.

[6] C. Chou, Y. Chen, D. Pham, and V. Truong, "Steel braced frames with dual-core SCBs and sandwiched BRBs: Mechanics modeling and seismic demands", *Engineering Structures*, vol. 72, pp. 26–40, 2014, doi: 10.1016/j.engstruct.2014.04.022.

[7] H. Wu, "Effects of restraining ratio on hysteretic performance of concrete-filled steel tube buckling-restrained braces", M.A. thesis, Harbin Institute of Technology, 2015.

[8] Y. Guo and X. Wang, "Bolt connection behavior and design of a four-angle assembled steel buckling-restrained brace: theoretical analysis", *Engineering Mechanics*, vol. 31, no. 1, pp. 56–63, 2014, doi: 10.6052/j.issn.1000-4750.2013.01.0004.

[9] X. Wang and Y. Guo, "Bolt connection behavior and design of a four-angle assembled steel buckling-restrained brace: numerical analysis", *Engineering Mechanics*, vol. 31, no. 2, pp. 15–24, 2014, doi: 10.6052/j.issn.1000-4750.2013.01.0005 .

[10] B. Zhu, Y. Guo, and Y. Yuan, "Load-carrying capacity and hysteretic performance of corrugated web connected BRB", *China Civil Engineering Journal*, vol. 51, no. 2, pp. 40–53, 2018, doi: 10.15951/j.tmgcxb.2018.02.005.

[11] M. Jia, F. Li, and B. Lu, "Experimental study on assembled buckling-restrained braces wrapped with carbon fiber", *Journal of Harbin Institute of Technology*, vol. 48, no. 6, pp. 98–104, 2016, doi: 10.11918/j.issn.0367-6234.2016.06.016.

[12] GB/T 228-2002 Metallic materials-Tensile testing at ambient temperature. China Architecture & Building Press, 2002.

[13] H. T. Zhao, G. Shi, Y. Gao, "Experimental study on cyclic behaviour of low yield point steel buckling-restrained braces", *Engineering Structures*, vol. 277, art. no. 115464, 2023, doi: 10.1016/j.engstruct.2022.115464.

[14] J. Z. Tong, E. Y. Zhang, Y. L. Guo, and C. Q. You, "Cyclic experiments and global buckling design of steel-angle-assembled buckling-restrained braces", *Bulletin of Earthquake Engineering*, vol. 20, no. 10, pp. 5107–5133, 2022, doi: 10.1007/s10518-022-01389-w.

[15] L. Gu, X. Gao and J. Xu, "Experimental research on seismic performance of BRB concrete frames", *Journal of Building Structures*, vol. 32, no. 7, pp. 101–111, 2011, doi: 10.14006/j.jzjgxb.2011.07.015.